Journal of the European Ceramic Society **19** (1999) 1705–1715
© 1999 Elsevier Science Limited
Printed in Great Britain. All rights reserved
PII: S0955-2219(98)00281-7
0955-2219/99/$ - see front matter

Fatigue and Fracture Characteristics of a Fine-grained (Mg,Y)–PSZ Zirconia Ceramic

R. Fernàndez,[a] F. Meschke,[b] G. De Portu,[c] M. Anglada[a] and L. Llanes[a,*]

[a]Departament de Ciència dels Materials i Engenyeria Metal.lúrgica, ETSEIB, Universitat Politècnica de Catalunya, Barcelona 08028, Spain
[b]Research Center Juelich, IWE-1, SOFC, Juelich 52425, Germany
[c]National Research Council, Research Institute for Ceramics Technology, Faenza 48018, Italy

(Received 7 August 1998; accepted 11 November 1998)

Abstract

The fatigue and fracture characteristics of a partially-stabilized fine-grained zirconia with spinel additions, (Mg,Y)–PSZ, were studied. Fracture toughness, crack growth resistance curves and fatigue crack growth (FCG) behavior, under both sustained and cyclic loading, were evaluated. Mechanical fatigue effects were clearly evidenced by (1) remarkable crack growth rate differences under cyclic and static loading and (2) significant loading ratio effects. Comparing the cyclic and the static FCG behavior allows to deduce a higher cyclic fatigue sensitivity of the fine-grained (Mg,Y)–PSZ with respect to a commercial peak-aged Mg–PSZ used as a reference material. By in situ *observation of crack extension under cyclic loading, the fatigue mechanisms could be resolved. Mechanical degradation of bridging ligaments, as already known for coarse-grained Mg–PSZ, is one source of cyclic fatigue. An additional source attributed to the particle dispersed microstructure of the (Mg,Y)–PSZ is the interaction between crack faces and hard spinel particles. The sensitivity of (Mg,Y)–PSZ and Mg–PSZ to cyclic fatigue is discussed in terms of the respective microstructures, prevalence and operativity of distinct mechanical fatigue mechanisms.* © *1999 Elsevier Science Limited. All rights reserved*

Keywords: PSZ, fatigue, racture, toughness, ZrO_2.

1 Introduction

Zirconia ceramics are candidate materials for a wide range of structural applications where improved and consistent performance together with high reliability are demanded. It is directly associated with their pronounced rising crack growth resistance with increasing crack size, namely *R*-curve behavior, mainly as a consequence of the large transformation toughening capability that they exhibit. This imparts these ceramics with the highly desirable property of 'flaw tolerance', i.e. their strength is independent of initial flaw size or subsequent in-service damage.[1,2]

The above statements are particularly true for MgO–partially stabilized zirconia (Mg–PSZ). For this system, a large number of investigations conducted over the last two decades has led to optimal processing routes and, as a result, to significant improvements in its relative fracture toughness and *R*-curve behavior (e.g. Refs 3–6). However, similar achievements have not been accomplished when considering other important structural characteristics of Mg–PSZ, e.g. maximum long-term application temperature. With respect to this parameter, it is well known that this material shows pronounced mechanical degradation when exposed at temperatures above 900°C, mainly as a consequence of the subeutectoid decomposition promoted in the MgO–ZrO_2 system.[3,7–10] This decomposition is highly localized on grain boundaries and may induce microcracking at them because the significant thermal expansion mismatch between the cubic matrix and the eutectoid product.[3,8,10]

In order to overcome the above impairment of Mg–PSZ, literature results indicate the addition of yttria as an alternative, particularly operative in terms of suppressing the subeutectoid decomposition up to temperatures about 1250°C.[11,12] Following that approach, Meschke *et al.* [13–16] have developed a zirconia partially stabilized with Y_2O_3 and MgO, which includes small amounts (3 vol%) of $MgAl_2O_4$ spinel particles. The resulting material,

*To whom correspondence should be addressed.

referred to as (Mg,Y)–PSZ, is a fine-grained (mean grain size below 15 μm) material that exhibits, after appropriate aging treatments, not only similar hydrothermal stability, toughening capability and corrosion resistance as conventional coarse-grained Mg–PSZ, but also better high temperature phase stability and higher flexural strength, under peak-aged conditions, than the latter material.[14–17]

On the other hand, many structural applications for which (Mg,Y)–PSZ could be intended to use include variable stresses too. Therefore, for design purposes as well as for estimation of reliability, in addition to the thermomechanical and environmental characteristics cited above, the resistance to fatigue crack propagation may also be of primary importance.

Cyclic degradation phenomena in PSZs were first confirmed about 10 years ago.[18,19] Since then, numerous investigations on the fatigue of these materials, mainly of Mg–PSZ, have been carried out experimentally and theoretically by many researchers. Extensive literature surveys on the fatigue behavior of Mg–PSZ have been presented, e.g. in Refs. 20–22, and the interested reader is referred to them for detailed information. Here, only some experimental facts on the fatigue crack growth (FCG) characteristics of Mg–PSZ will be briefly reviewed.

From the mechanics standpoint, it is now well known that for Mg–PSZ: (1) crack growth rates for a given maximum applied stress intensity factor (K_{max}) are higher under cyclic loads than under a constant one; and (2) there is a very large power-law dependence of crack growth rates of long sharp cracks on K_{max} (or ΔK).[10,18,20,23–27] Further, such relationships are strongly affected by extrinsic (environment, temperature, load ratio, etc.)[24,25] as well as intrinsic (phase transformation capability, microstructure, etc.) factors.[10,20,24,26,27] On the other hand, from the mechanisms viewpoint, several cyclic-induced phenomena have been postulated in association with cyclic fatigue of Mg–PSZ. The proposed processes include: slip line formation [25] and microcracking [21] at the crack tip; bridging degradation, of both ligaments [22,24,27,28] and precipitates, [22,28] at the crack wake; and transformation toughening reversibility. [21] However, there is not conclusive experimental evidence for identifying any of them as consistently responsible for the mechanical fatigue effects observed. Taking into consideration the experimental facts presented for each mechanism in the corresponding studies, it seems more concordant to describe the mechanical fatigue in these materials as the result of a complex interactive effect of all, or at least some, of them than on the basis of a particular phenomenon.

It is the aim of this study to investigate and to establish the cyclic and the static FCG behavior, i.e. that related to subcritical crack growth by true mechanical fatigue and environmentally-assisted degradation respectively, of a fine-grained zirconia with spinel additions, (Mg,Y)–PSZ. Of particular interest is the investigation of how microstructural characteristics affect the relative cyclic to static FCG behavior of (Mg,Y)–PSZ, as compared to that previously reported by the authors for a conventional coarse-grained Mg–PSZ (FZM type, 3 wt% MgO, Friatec AG, Mannheim, Germany).

2 Experimental Procedure

2.1 Sample preparation

The material studied was a fine-grained zirconia, co-stabilized with magnesia and yttria, with spinel additions, (Mg,Y)–PSZ. Samples were prepared from mixtures of commercial stabilized zirconia powders (final stabilizer contents of 0·5 Mol% Y_2O_3 and 7·8 mol% MgO). An amount corresponding to 3 vol% of $MgAl_2O_4$ spinel particles was added to the composition. This mixture was attrition milled in ethanol in a polyethylene-lined recipient. After wet sieving and rotovap drying, the powder was sieved with a 140-μm grid.

Powder compacts were prepared by uniaxial pressing at 31 MPa followed by cold isostatic pressing at 500 MPa. Green bodies with a density of 55% of the theoretical one were sintered in air at 1720°C for 30 min, rapidly cooled to 1400°C, isothermally held for 60 min, and finally quenched to room temperature. From the 4 mm thick blocks obtained, rectangular prisms were cut and rectified.

2.2 Microstructural examination

Samples for analysis by optical (OM) and scanning electron microscopy (SEM) were prepared by polishing sectioned pieces of the rectangular prisms. They were then etched at room temperature in concentrated HF for 4 min. Microstructural features were examined using a JEOL JMS6400 microscope. Transmission electron microscopy (TEM) samples were also prepared. Thin foils were cut and mechanically ground to 100 µm. Disks (3 mm in diameter) were cut from the thin foils of material using an ultrasonic drill. The disks were then dimple-polished to 30 μm center thickness and ion milled. A thin film of carbon was evaporated onto the foil to avoid charging while under the electron beam. A 120-KV JEOL 1200EXII microscope was used for TEM.

2.3 Mechanical characterization

Fracture strength was measured at room temperature on unnotched beams of 4×4×30 mm dimensions. A fully articulating four-point bend test jig

(inner span 11·5 mm, outer span 23 mm) was used. The specimens were first polished on the surface which was later subjected to the maximum stress in bending. Polishing was conducted using diamond pastes of 30 and 6 μm and colloidal silica as a final step. The edges of the polished samples were slightly chamfered for the flexural strength tests.

Fracture toughness, crack growth resistance curve (*R*-curve) and FCG behavior were measured under four-point bending and using single edge-notch beams (SENB) of $4\times7\times30$ mm dimensions with a notch length-to-specimen width ratio (a/w) of 0·3. The specimens were first pre-cracked by cyclic compression in an Instron servo-hydraulic testing machine (model 1341). Loading conditions during the pre-cracking procedure included: sine waveform, load ratio (R) of 10, testing frequency of 20 Hz and minimum applied stress between 300 and 380 MPa. The resulting cracks were usually about 50 to 150 μm long, after 10^5 to 10^6 cycles, and were associated with extensive degradation together with an extremely rough appearance. In order to avoid possible pre-cracking and crack-tip geometry effects,[29] these cracks were further propagated about 120 μm, under far-field tensile loads, before carrying out any subsequent crack growth resistance testing.

Fracture toughness and *R*-curve behavior were determined following a direct-measurement method. Tests were run under crack opening displacement (COD) control in an Instron servo-hydraulic testing machine (model 8511). The imposed COD ramp was of 0·1 μm s^{-1}. Load values were computer-recorded with a data acquisition rate of 10 points/s. Stable crack extension was monitored *in situ* with an accuracy of $\pm 5\,\mu$m using a long-range telescope Questar (model QM100). In order to facilitate crack extension measurement, the lateral faces of the SENB specimens were previously polished. The characteristic *R*-curve (K_{appiied} versus crack length) was finally assembled from the simultaneously collected data series of load-time and crack length-time, using the stress intensity factor expression for SENB geometry as given by Tada *et al.*[30] Fracture toughness was determined as the plateau value of the measured *R*-curve.

FCG under cyclic loading was evaluated at a frequency of 2 Hz under load control using a sine waveform and R values of 0·2 and 0·6. For comparison, environmentally assisted or static FCG was measured with specimens subjected to constant applied load. The load value was that corresponding to a resulting K_{applied} equal to the $K_{\max}$ value experienced by the sample under cyclic loading. It was reached following an initial ramp of 100 N s^{-1}. As before, and for both loading conditions, stable crack growth was measured *in situ* using a long-range telescope. All tests were carried out at room temperature and humidity of about 55%.

Fractographic aspects associated with different loading conditions were documented either from *in-situ* examination, using the long-range optical microscope, or by investigating the fracture surfaces of broken samples through OM and SEM.

3 Results and Discussion

3.1 Microstructure

The average grain size, as obtained from OM and SEM images, was about 12 μm (Fig. 1). Grain size differences between the material studied and commercial Mg–PSZ is attributed to the addition of spinel particles (of size between 1 and 5 μm) and their effect on hindering grain growth. A SEM and TEM examination allowed to discern a common PSZ microstructure, i.e. orthogonally oriented oblate precipitates immersed in a cubic matrix. The volume fraction of thin ellipsoidal second-phase particles was about 40%. Those of size over 150 nm showed a twinned aspect and monoclinic symmetry, whereas precipitates smaller than 100 nm had a tetragonal symmetry. The precipitate size distribution was highly heterogeneous, as shown in Fig. 2. As clearly discerned by TEM (Fig. 3.) zones close to spinel particles were often characterized by less numerous precipitates but of sizes larger than the corresponding mean values. The pronounced heterogeneity observed for the precipitate size distribution together with the existence of spinel particles in (Mg,Y)–PSZ will be two important microstructural features to consider when comparing the mechanical behavior of this material with that of a peak-aged Mg–PSZ previously investigated by the authors.

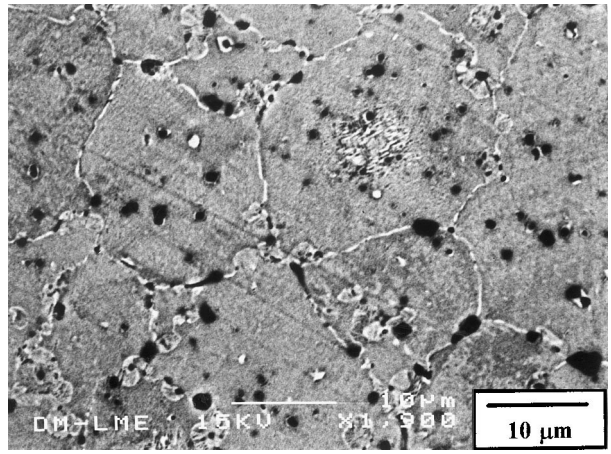

Fig. 1. SEM image showing microstructural features of (Mg,Y)–PSZ. Black spots correspond to spinel particles.

3.2 Mechanical characteristics

3.2.1 Flexural strength and fracture toughness

The mean flexural strength of the material studied was of 678 MPa (±45 MPa), about 40% higher than that previously found by the authors for a commercial coarse-grained Mg–PSZ under peak-aged conditions, i.e. with maximum fracture toughness.[10] The higher measured strength for the (Mg,Y)–PSZ must be directly associated with the lower processing flaw size resulting of the grain size reduction.[15,16]

Fracture toughness, *R*-curve and FCG behavior were evaluated using SENB specimens with sharp cracks obtained first under cyclic compression loading and subsequently extended under far-field tensile loads. The cyclic compression pre-cracking procedure yields residual tensile stresses at the tip of the notch upon unloading from the maximum far-field compression stress.[31] It finally resulted, before further propagation of the obtained pre-cracks, in pronounced fatigue damage at the bottom of the notch, as clearly shown in Fig. 4. Particular fractographic features were also found as related to the cyclic compression pre-cracking procedure. Figure 5 shows an example of the indentation-like impressions (arrow) usually found on fracture surfaces corresponding to the precracking zone. Their morphological aspect and microstructural dimensions suggest such impressions as being produced as a consequence of hard spinel particles smashing against the fine-grained structure during the cyclic compression procedure. Hence, it is proposed that wedging effects associated with the interaction between crack faces and spinel particles may also exist, under cyclic loading, just behind the crack tip for the material studied. The relative influence of such effects on the mechanical characteristics of (Mg,Y)–PSZ will be discussed later.

Fracture toughness plateau value for the (Mg,Y)–PSZ was 9·8 MPa$\sqrt{m}$ (±0·4 MPa$\sqrt{m}$). It was about 10% higher than that of the peak-aged Mg–PSZ studied before. Figure 6 shows the measured *R*-curve. It may be described as very

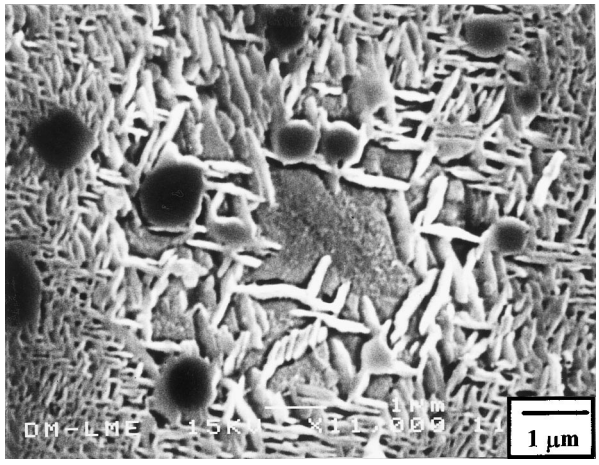

Fig. 2. SEM micrograph showing details of the precipitate size distribution within a grain of (Mg,Y)–PSZ.

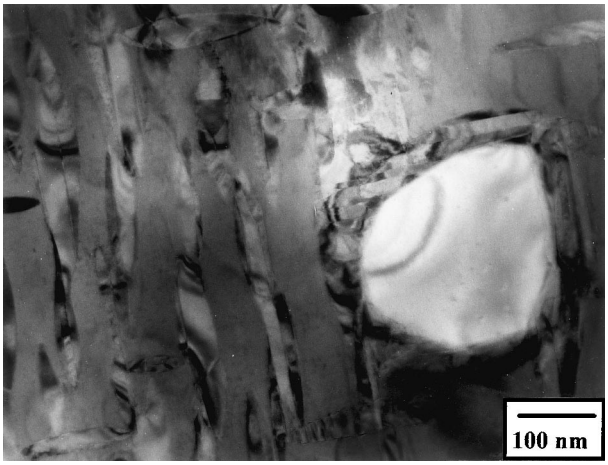

Fig. 3. Bright-field TEM image showing regions of low density but very large monoclinic precipitates near spinel particles.

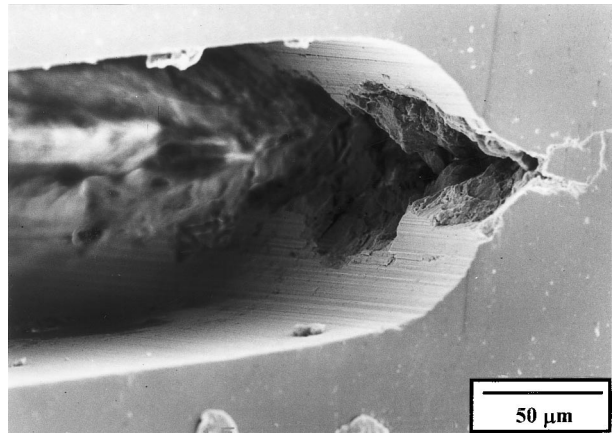

Fig. 4. SEM image showing fatigue damage at the bottom of the notch in a sample pre-cracked under cyclic compression loading.

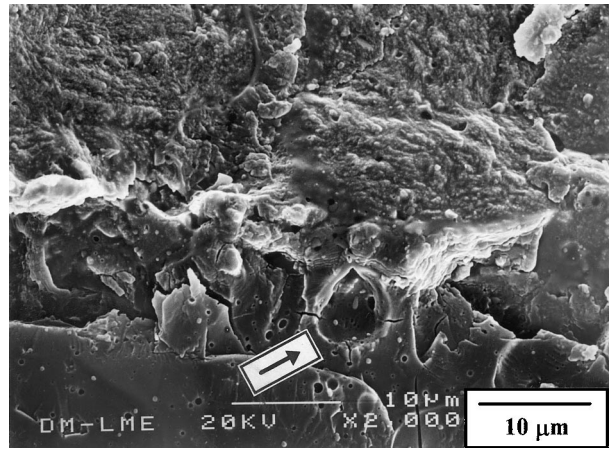

Fig. 5. Fracture surface corresponding to the pre-cracked zone of a tested sample. The indentation-like impression (arrow) is suggested to be produced by the mechanical interaction between crack faces and spinel particles during the pre-cracking procedure.

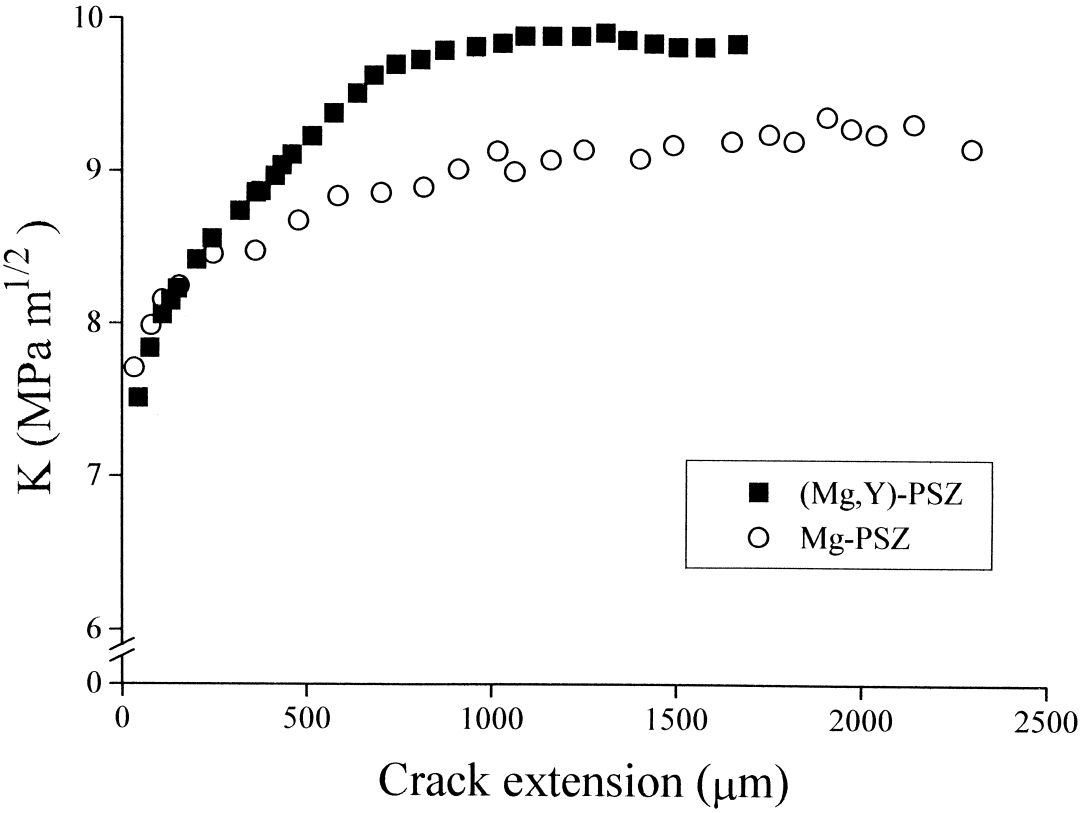

Fig. 6. Experimentally determined *R*-curve for the fine-grained (Mg,Y)–PSZ. The corresponding *R*-curve for a peak-aged coarse-grained Mg–PSZ[32] is also shown for comparative purposes.

pronounced and developing over a crack extension of about 1 mm. In that figure, the *R*-curve of the Mg–PSZ used as reference in this investigation [32] is also shown for comparative purposes. Crack growth rates during the *R*-curve measurements for both materials were experimentally determined to be in the range of 2×10^{-5} to 2×10^{-4} m/s^{-1}, i.e. high enough to neglect any possible environmental assisted cracking effects, as concluded from the static fatigue results to be presented in the next section.

The qualitatively alike raising *R*-curves indicate that both materials exhibit similar main toughening mechanisms. Experimental observations confirm crack shielding by transformation of the transgranularly distributed precipitates as the main toughening mechanism for both materials. The referred experimental findings were: (1) a large volume fraction of highly metastable tetragonal zirconia precipitates, a feature already reported in a previous work;[16] (2) surface rumpling during crack propagation; and (3) relatively large crack extension in which the plateau values were achieved. However, other toughening mechanisms such as precipitate or uncracked ligament bridging may also be active.[20,22,27,28] Whereas differences with respect to toughening effectivity are not expected for the precipitate bridging mode, because of the similar mean size value of the transforming precipitates in both materials; they could exist for the ligament mode due to the more heterogeneous microstructure of the (Mg,Y)–PSZ. The optical resolution of the *in-situ* crack growth monitoring technique used in this investigation did allow to evidence the ligament bridging but not the precipitate one. Uncracked ligaments of size ranging from 5 to 30 μm were clearly observed during crack growth. Their occurrence was, at least from lateral surface observations, more widespread in the fine-grained PSZ than previously found in the coarse-grained one. Following Moller *et al.*'s [28] and Hoffman *et al.*'s [22,27] findings, it is suggested that this larger prevalence of uncracked ligaments in the fine-grained PSZ must be a direct consequence of the similarly higher fraction of large monoclinic precipitates in this material. These precipitates are believed to favor, under the stress field associated with the incoming crack, radial cracking and then bridging ligament formation. Hence, the differences in the *R*-curves between the two PSZs referred in this investigation, particularly in terms of fracture toughness plateau value, seem to be related to a more prominent effect from uncracked ligament bridging in the (Mg,Y)–PSZ as a complementary toughening mechanism of the one resulting from the stress-induced transformation of tetragonal precipitates.

3.2.2 Fatigue crack growth

FCG behavior for the (Mg,Y)–PSZ is shown in Fig. 7. The crack growth rate (da/dt) data was

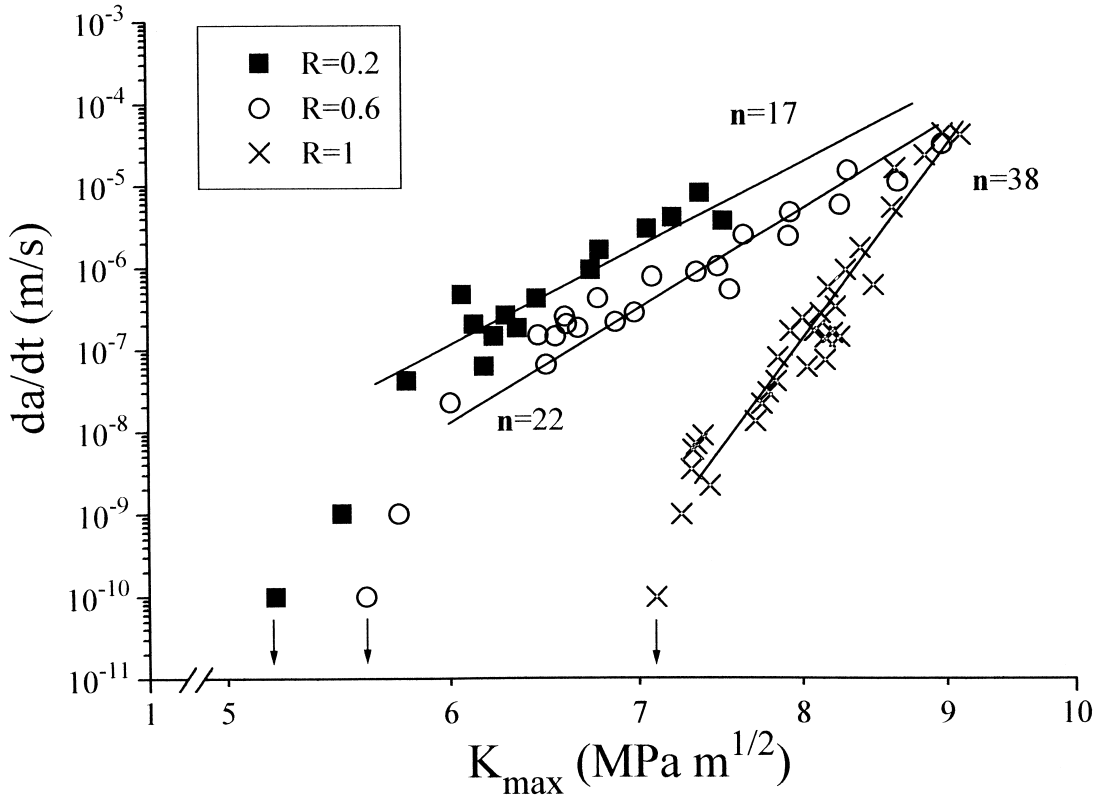

Fig. 7. Crack growth rate as a function of maximum applied stress intensity factor (K_{max}) for (Mg,Y)–PSZ and for each loading condition studied. The corresponding Paris coefficients are given by n and dropping arrows represent the highest K_{max} for which crack growth was not noticed after 50 000 s.

plotted in terms of maximum applied stress intensity factor (K_{max}) in order to include results from static fatigue testing, i.e. that conducted at $R=1$. Crack growth thresholds were attained following an incremental loading sequence corresponding to $0{\cdot}1\,MPa\sqrt{m}$ steps. Threshold values were defined as the K_{max} associated with a da/dt of $10^{-9}\,m\,s^{-1}$. A power-law dependence, $(da/dt)=AK_{max}^{n}$, i.e. a Paris-like relationship, was obtained in all cases in the range of crack growth rates between 10^{-8} and $10^{-4}\,m\,s^{-1}$.

Remarkable crack growth rate differences were found under cyclic and static loading conditions. Like in a previous work for other advanced zirconia-based ceramics,[10] crack growth threshold and the (Paris) exponent in the power-law dependence were higher under static than under cyclic loading. The corresponding absolute values are given in Table 1 for each loading condition studied. A clear load ratio effect, for values between 0·2 and 1, was measured. The trend showed by these experimental findings indicates by itself the existence of true mechanical fatigue. Damage was also evident through in situ observation of degradation of bridges formed by uncracked ligaments during crack growth under cyclic loads (Fig. 8). The development and subsequent rupture of these bridging ligaments was exclusively observed in the surface; however, the relationship crack extension–applied load as well as the fractographic features allow to point out the phenomenon as occurring across the through-thickness crack front at various stages. Following previous studies on cyclic fatigue of coarse-grained Mg–PSZ[20,22,24,27,28,33–35] it is stated that cyclic fatigue

Table 1. Crack growth threshold and Paris exponent in the power-law dependence, $(da/dt)=AK_{max}^{n}$, for fine-grained (Mg,Y)–PSZ and for each loading condition studied

Loading ratio (R)	*Fatigue crack growth threshold* [K_{th} ($MPa\sqrt{m}$)]	*Paris exponent* (n)
1	7·0	38
0·6	5·7	22
0·2	5·1	17

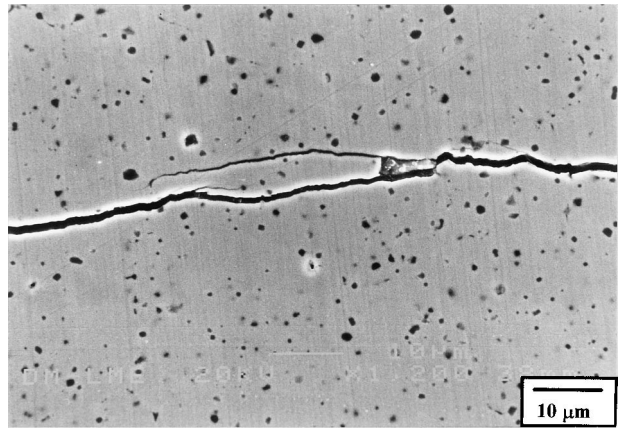

Fig. 8. SEM image showing a typical uncracked ligament developed in (Mg,Y)–PSZ during stable fatigue crack growth.

effects in PSZ are associated with degradation of not only ligament bridging but also precipitate bridging (possibly the most important one[22,28]) and localized microplasticity or microcracking at the crack tip. However, clear in-situ evidence of the latter processes was impossible to obtain within the optical microscope range used in this investigation.

Transgranular fracture was always observed regardless of the applied loading condition. The fracture surface of a sample tested under cyclic loading, within the stable crack propagation zone, is shown in Fig. 9. Here, polyhedral spinel particles

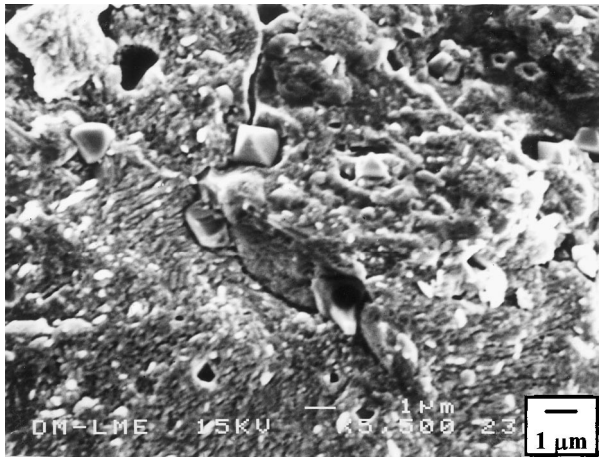

Fig. 9. SEM micrograph showing transgranular fracture and exposed spinel particles under stable crack propagation in (Mg,Y)–PSZ.

or holes of similar morphology are clearly seen, indicating that cracks usually went around particles during stable propagation. This observation is very interesting because it points out the feasibility of a particle–crack face interaction similar to that previously found under cyclic compression loading. It is then suggested that during stable crack propagation, at stress levels associated with small crack tip opening, such interaction may promote wedging effects that could result in an additional cyclic fatigue degradation mechanism in (Mg,Y)–PSZ. On the other hand, unstable crack propagation areas showed a higher fraction of cleaved particles. The fact that different particle–crack fracture interactions are dominant at low and high applied stress intensity factors pinpoints the relative importance of parameters such as specific interface fracture energy and particle size in determining the fracture characteristics of the material studied.

3.3 Relative cyclic to static fatigue behavior

Following the results above presented for the (Mg,Y)–PSZ, in this section it is attempted to discuss the cyclic and static fatigue behavior of this material as compared to that previously found by the authors for a commercial peak-aged Mg–PSZ.[10] The observed trends for R values of 0·2 and 1 in both materials are shown in Fig. 10. Clearly, environmental-assisted crack growth rates are much higher, for a given applied K_{max}, for the

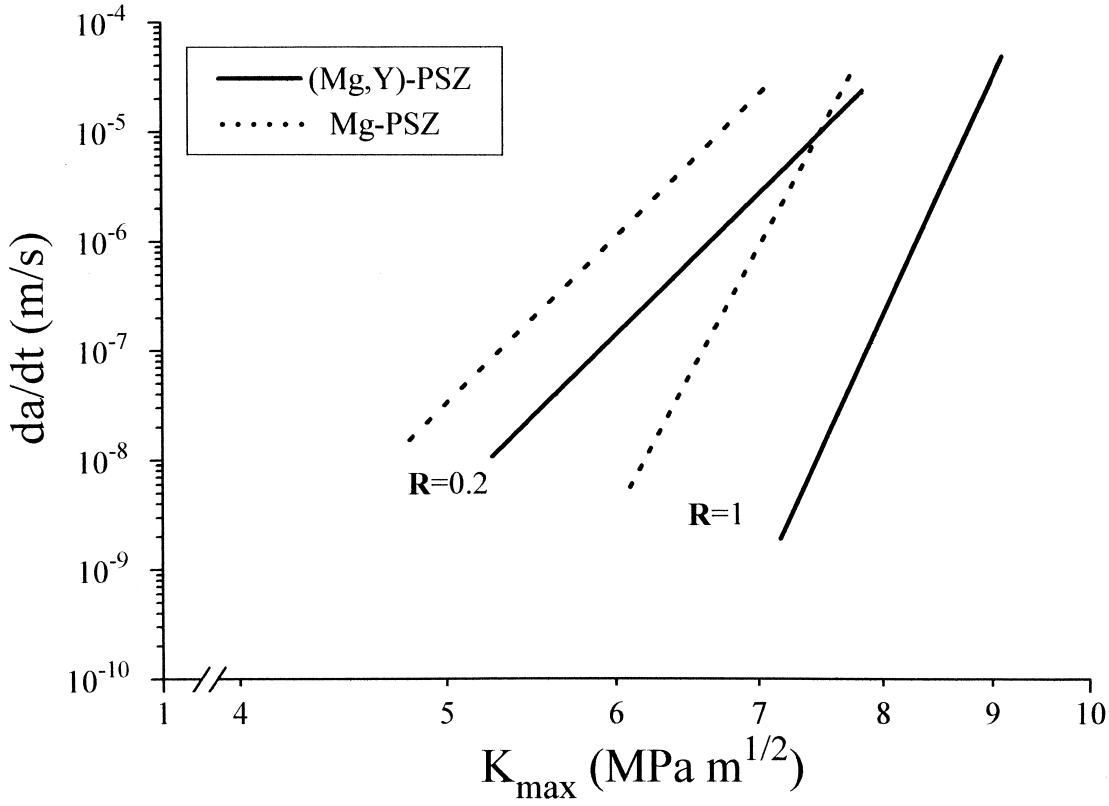

Fig. 10. Experimental data trends corresponding to the FCG behavior of fine-grained (Mg,Y)–PSZ and a coarse-grained Mg–PSZ used as a reference, [10,32] both at peak-aged conditions, under cyclic ($R=0{\cdot}2$) and constant ($R=1$) applied loading.

coarse-grained material than for the fine-grained one, pointing out the higher static fatigue crack growth resistance of the (Mg,Y)–PSZ. On the other hand, the differences between the corresponding rates under cyclic loading conditions are much less pronounced. This observation, once the corresponding static fatigue effects are considered, indicates a different cyclic to static fatigue behavior for both materials.

The fact that crack growth under cyclic loading in ceramics is a cojoint effect of environmental action and (possible) mechanical fatigue degradation leads to evaluate their fatigue behavior, particularly for comparison purposes among different materials, in terms of rather relative cyclic to static fatigue effects. Accordingly, in this investigation one parameter is proposed which intends to weigh the reduction in resistance to crack growth due to mechanical fatigue. It is then used for evaluating and comparing the true cyclic fatigue crack propagation behavior of the two different PSZs.

This parameter, termed as ϕ_C, is associated with the real mechanical fatigue effects involved during crack growth under cyclic loading. It is defined as the ratio between the experimentally determined threshold value ($K_{th,c}$) and that estimated considering environmental-related degradation to occur exclusively under cyclic loading ($K_{th,ce}$), i.e. $\phi_C = (K_{th,c}/K_{th,ce})$. The cyclic crack growth rate, assuming that there is not any mechanical fatigue, is calculated from the experimentally measured static fatigue data, following the guidelines given by Evans and Fuller.[36] Under these conditions, crack growth rates related to cyclic loading are estimated to diminish for a given maximum applied stress intensity factor. The decreasing amount would depend upon the exponent coefficient fitted in the corresponding power-law dependence obtained for the static fatigue experience.

Figure 11 shows the relative positions of the experimental and estimated data for (Mg,Y)–PSZ. From that figure, the existence of true mechanical fatigue effects in this material is even reinforced. Similar trend is found for Mg–PSZ. The calculated ϕ_C values for the fine- and coarse-grained PSZs are 0·69 and 0·76 respectively. Based upon the physical meaning of the parameter ϕ_C, the higher its value, the lower the material sensitivity to real mechanical fatigue degradation. Hence, it is concluded that the fine-grained material exhibits a lower intrinsic cyclic fatigue resistance to crack growth than the coarse-grained one, although the former has a higher static fatigue resistance to crack growth than the latter. However, the differences are relatively small when compared with those determined for Y–TZP,[37] a material whose behavior is strongly affected by the environment.[29] Such slender variations between the rationalized behaviors of (Mg,Y)–PSZ and Mg–PSZ are expected, once the PSZ character of both materials is considered.

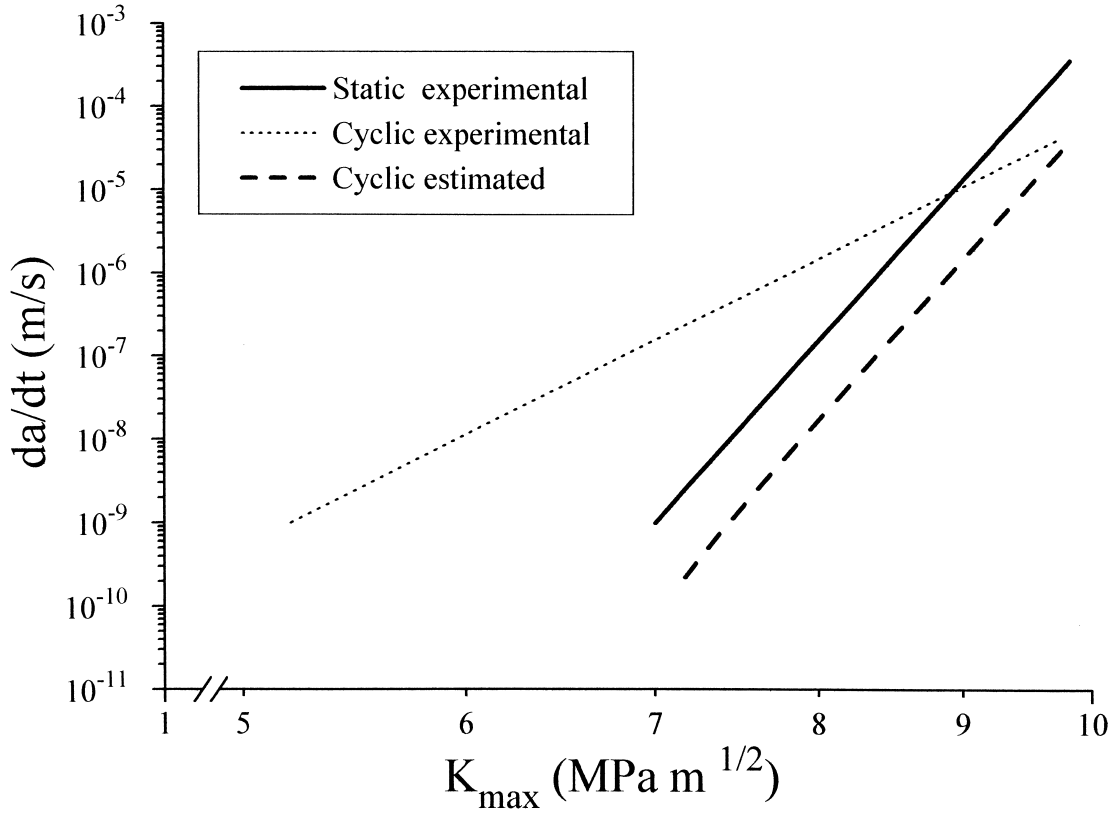

Fig. 11. Schematic graph showing relative positioning of experimental and estimated crack growth rate versus K_{max} data under cyclic and static loading conditions.

The lower ϕ_C value, or the higher mechanical fatigue sensitivity, found for the fine-grained PSZ as compared to the coarse-grained one should be related to differences on the degradation mechanisms of both materials. The identification of cyclic fatigue mechanisms in PSZ has been a subject that, although widely studied, has not still provided clear and unique conclusions. Thus, mechanisms as distinct as localized microplasticity or microcracking at the crack tip, transformation toughening reversibility, and precipitate and ligament bridging degradation have been proposed. From all of them, as previously discussed for the fracture toughness results, uncracked ligament bridging seems to be the only one in which noticeable differences, in relative terms, can be addressed between both PSZs. On the other hand, interactions between spinel particles and crack faces could induce another cyclic degradation mechanism in the (Mg,Y)–PSZ. Both cases are discussed below.

The microstructure of the fine-grained (Mg,Y)–PSZ was much more heterogeneous, in terms of both precipitate size distribution and volume fraction of large monoclinic precipitates, than that of the coarse-grained PSZ. On the other hand, the number of crack-bridges involving uncracked ligaments was also significantly higher in the former material than in the latter one. These two observations, following Hoffman *et al.*'s ideas ,[22] are closely related by means of large monoclinic precipitates acting indirectly as seeds for developing the corresponding bridges. Cyclic degradation of these bridges was clearly identified by *in situ* observation during crack growth, and as a consequence, surface crack growth rates were enhanced. Thus, the more widespread finding of those uncracked ligaments in (Mg,Y)–PSZ than in Mg–PSZ would indicate a similarly more pronounced mechanical fatigue effect, as observed. Although this approach has initially been postulated by Hoffman *et al.* [22] in attempting to explain a higher prevalence of erratic FCG behavior in larger cubic grain size Mg-PSZs observed in a previous work, [27] the dependence of mechanical fatigue effects on frequency of uncracked ligaments is difficult to discern from their experimental results, mainly because they correspond to materials with quite different intrinsic fracture toughness and do not include crack growth data under sustained loading for all the conditions studied.

In order to attain a fine-grained microstructure hard spinel particles were added to the material here studied. Following experimental evidences such as those shown in Fig. 6, it is suggested that those particles may interact with crack faces, and hence, provide a particular mechanical fatigue mechanism in terms of wedging effects developing during the unloading portion of a cycle due to crack closure. Such particle-crack faces interaction may induce, as previously postulated for fatigue crack growth in silicon nitride,[38] nucleation and growth of microcracks at the crack tip; and thus, a more pronounced mechanical fatigue effect in the fine-grained (plus hard spinel particles) structure than in the coarse-grained (without any second phase particles) one. This mechanism is then suggested to be a complementary reason for the higher relative cyclic fatigue degradation observed for (Mg,Y)–PSZ as compared to the conventional Mg–PSZ previously studied.

4 Conclusions

The fracture and fatigue characteristics of a fine-grained (Mg,Y)-PSZ have been investigated. On the basis of the experimental findings the following conclusions can be drawn:

1. The addition of spinel particles to partially stabilized zirconia not only hinders grain growth but also strongly affects the intrinsic precipitate size distribution, particularly in terms of fraction of large monoclinic precipitates.
2. The fine-grained (Mg,Y)–PSZ showed a higher flexural strength than that of a commercial peak-aged Mg–PSZ used as reference, but without affecting the toughness-related behavior, i.e. the material exhibited similar high fracture toughness plateau value and pronounced *R*-curve as those usually reported for Mg–PSZ.
3. As previously found for other PSZ materials, fine-grained (Mg,Y)–PSZ clearly displays true mechanical fatigue effects. Further, once environmental assisted cracking under sustained load is considered, they are found to be more pronounced than those determined for a reference coarse-grained Mg–PSZ. However, even if its mechanical fatigue sensivity is higher, (Mg,Y)–PSZ exhibits also higher crack growth resistance than the conventional Mg–PSZ, particularly under static fatigue conditions.
4. The higher mechanical fatigue sensitivity of the (Mg,Y)–PSZ, as compared to that of a conventional Mg–PSZ, is related to: (1) a larger prevalence of uncracked ligament bridging; and hence, a more pronounced effect associated with its degradation under cyclic loading; and (2) the existence of particular wedging effects in terms of interactions between crack faces and hard spinel particles

in the crack wake which finally result in another operative cyclic degradation process at the crack tip.

Acknowledgements

This work was supported by the Spanish Comisión Interministerial de Ciencia y Tecnologia (CICYT) under grant MAT94-0431. The authors gratefully acknowledge this generous support and also thank M. Marsal, J. M. Manero, and D. Casellas for experimental and analytical assistance in this work. Likewise, one of the authors (R.F.) would like to express his gratitude for the scholarship received from the Instituto de Cooperación Iberoamericana (ICI).

References

1. Cook, R. F., Lawn, B. R. and Fairbanks, C. J., Microstructure-strength properties in ceramics: I, Effect of crack size on toughness. *J. Am. Ceram. Soc.*, 1985, **68**, 604–615.
2. Bennison, S. J. and Lawn, B. R., Flaw tolerance in ceramics with rising crack-resistance characteristics. *J. Mater. Sci.*, 1989, **24**, 3169–3175.
3. Porter, D. L. and Heuer, A. H., Microstructural development in MgO-partially stabilized zirconia (Mg–PSZ). *J. Am. Ceram. Soc.*, 1979, **62**, 298–305.
4. Hannink, R. H. and Swain, M. V., Magnesia-partially stabilised zirconia: the influence of heat treatment on thermomechanical properties. *J. Aust. Ceram. Soc.*, 1983, **18**, 53–62.
5. Hughan, R. R. and Hannink, R. H., Precipitation during controlled cooling of magnesia–partially-stabilized zirconia. *J. Am. Ceram. Soc.*, 1986, **69**, 556–563.
6. Montross, Ch. S., Pro- and subeutectoid behavior of the tetragonal phase in magnesia–partially-stabilized zirconia. *J. Am. Ceram. Soc.*, 1992, **75**, 463–468..
7. Swain, M. V., Garvie, R. C. and Hannink, R. H. J., Influence of thermal decomposition on the mechanical properties of magnesia-stabilized cubic zirconia. *J. Am. Ceram. Soc.*, 1983, **66**, 358–362.
8. Hannink, R. H. J., Microstructure development of subeutectoid aged MgO–ZrO_2 alloys. *J. Mater. Sci.*, 1983, **18**, 457–470.
9. Farmer, S. C., Heuer, A. H. and Hannink, R. H. J., Eutectoid decomposition of MgO-partiallystabilized ZrO_2. *J. Am. Ceram. Soc.*, 1987, **70**, 431–440.
10. Nagl, M. M., Llanes, L., Fernández, R. and Anglada, M., The fatigue behavior of Mg–PSZ and ZTA ceramics. In *Fracture Mechanics of Ceramics 12: Fatigue, Composites and High Temperature Behavior*, ed. R. C. Bradt, D. P. H. Hasselman, D. Munz, M. Sakai and V.Ya. Shevchenko. Plenum Press, New York, 1996, pp. 61–76.
11. Scott, H. G., Phase relationships in the magnesia–yttria–zirconia system. *J. Aust. Ceram. Soc.*, 1981, **17**, 16–20.
12. Dworak, U., Olapinski, H. and Burger, W., Thermal stability of PSZ. In *Advances in Ceramics Vol. 24a: Science and Technology of Zirconia III*, ed. S. Somiya, N. Yamamoto and H. Yanagida. American Ceramic Society, Columbus, OH, 1988, pp. 545–548.
13. Meschke, R, De Portu, G. and Claussen, N., Microstructure and thermal stability of finegrained (Y,Mg)–PSZ ceramics with alumina additions. *J. Eur. Ceram. Soc.*, 1993, **11**, 481–486.
14. Meschke, F., De Portu, G. and Claussen, N., Preparation and characterization of fine-grained (Mg,Y)–PSZ ceramics with spinel additions. In *Science and Technology of Zirconia V*, ed. S. P. S. Badwal, M. J. Bannister and R. H. J. Hannink. Technomic Publishing, Lancaster, PA, 1993, pp. 378–385
15. Meschke, R, Claussen, N., De Portu, G. and Rödel, J., Phase stability of fine-grained (Mg,Y)–PSZ. *J. Am. Ceram. Soc.*, 1995, **78**, 1997–1999.
16. Meschke, R, Claussen, N., De Portu, G. and Rödel, J., Preparation of high-strength (Mg,Y)–partially stabilised zirconia by hot isostatic pressing. *J. Eur. Ceram. Soc.*, 1997, **17**, 843–850.
17. Boukis, N., Claussen, N., Ebert, K., Janssen, R. and Schacht, M., Corrosion screening tests of high-performance ceramics in supercritical water containing oxygen and hydrochloric acid. *J. Eur. Ceram. Soc.*, 1997, **17**, 71–76.
18. Dauskardt, R. H., Yu, W. and Ritchie, R. O., Fatigue crack propagation in transformation toughened zirconia ceramic. *J. Am. Ceram. Soc.*, 1987, **70**, C248–C252.
19. Swain, M. V. and Zelizko, V., Comparison of static and cyclic fatigue on Mg–PSZ alloys. In *Advances in Ceramics Vol. 24b: Science and Technology of Zirconia III*, ed. S. Somiya, N. Yamamoto and H. Yanagida. American Ceramic Society, Columbus, OH, 1988, pp. 595–606.
20. Hoffman, M. J., Dauskardt, R. H., Mai, Y. -W and Ritchie, R. O., A review of the mechanics and mechanisms of cyclic fatigue-crack propagation in transformation-toughened zirconia ceramics. In *Science and Technology of Zirconia V*, ed. S. P. S. Badwal, M. J. Bannister and R. H. J. Hannink. Technomic Publishing, Lancaster, PA, 1993, pp. 321–38.
21. Chen, I. -W. and Liv, S. -Y., Constitutive relations for mechanical fatigue in zirconia ceramics. In *Fatigue of Advanced Materials*, ed. R. O. Ritchie, R. H. Dauskardt and B. N. Cox. Materials and Component Engineering. Publications, Edgbaston, UK, 1991, pp. 153–168.
22. Hoffman, M., Mai, Y. -W, Wakayama, S., Kawahara, M. and Kishi, T., Crack-tip degradation processes observed during in situ cyclic fatigue of partially stabilized zirconia. *J. Am. Ceram. Soc.*, 1995, **78**, 2801–2810.
23. Sylva, L. A. and Suresh, S., Crack growth in transforming ceramics under cyclic tension loads. *J. Mater. Sci.*, 1989, **24**, 1729–1738.
24. Dauskardt, R. H., Marshall, D. B. and Ritchie, R. O., Cyclic fatigue crack propagation in magnesia-partially-stabilized zirconia ceramics. *J. Am. Ceram. Soc.*, 1990, **73**, 893–903.
25. Davidson, D. L., Campbell, J. B. and Lankford, L., Fatigue crack growth through partially stabilized zirconia at ambient and elevated temperatures. *Acta Metall. Mater.*, 1991, **39**, 1319–1330.
26. Lathabai, S. and Hannink, R. H. J., Microstructure-crack resistance-fatigue correlations in eutectoid-aged Mg–PSZ. In *Science and Technology of Zirconia V*, ed. S. P. S. Badwal, M. J. Bannister and R. H. J. Hannink. Technomic Publishing, Lancaster, PA, 1993, pp. 360–370.
27. Hoffman, M. J., Mai, Y. -W, Dauskardt, R. H., Ager, J. and Ritchie, R. O., Grain size effects on cyclic fatigue and crack-growth resistance behaviour of partially stabilized zirconia. *J. Mater. Sci.*, 1995, **30**, 3291–3299.
28. Moller, C. V., Healy, J. C. and Mai, Y. -W., *In situ* scanning electron microscope observations of fatigue in magnesia–partially-stabilized zirconia. *Fatigue Fract. Engng Mater. Struct.*, 1994, **17**, 285–296.
29. Alcalá, J. and Anglada, M., Fatigue and static crack propagation in yttria-stabilized tetragonal zirconia polycrystals: crack growth micromechanisms and precracking effects. *J. Am. Ceram. Soc.*, 1997, **80**, 2759–2772.
30. Tada, H., Paris, P. C. and Irwin, G. R., The *Stress Analysis of Cracks Handbook*. Del Research Corporation, St. Louis, MO, 1973, pp. 2·13–2·15.

31. Suresh, S., *Fatigue of Materials*. Cambridge University Press, Cambridge, 1991, pp. 436–444.
32. Fernández, R., Llanes, L. and Anglada, M., Crecimiento de grietas por fatiga en la circona parcialmente estabilizada (Mg–PSZ). *Anales de Mecánica de la Fractura*, 1996, **13**, 209–214.
33. Jorgensen, M. H., Micro-mechanical modelling of crack bridging in ZTC. In *11th Riso International Symposium on Metallurgy and Materials Science*, ed. J. J. Bentzen, J. B. Bilde-Sorensen, N. Christiansen, H. Horsewell and B. Ralph. Riso National Laboratory, Roskilde, Denmark, 1990, pp. 353–358.
34. Dauskardt, R. H., Carter, W. C., Viers, D. K. and Ritchie, R. O., Transient subcritical crackgrowth behaviour in transformation toughened ceramics. *Acta Metall. Mater*., 1990, **38**, 2327–2336.
35. Steffen, A. A., Dauskardt, R. H. and Ritchie, R. O., Cyclic fatigue life and crack growth behavior of microstructurally small cracks in magnesia-partially-stabilized zirconia ceramics. *J. Am. Ceram. Soc*., 1991, **74**, 1259–1268.
36. Evans, A. G. and Fuller, E. R., Crack propagation in ceramic materials under cyclic loading conditions. *Metall. Trans*., 1974, **5**, 27–33.
37. Casellas, D., Fernández, R., Nagl. M.M., Alcalá, J., Llanes, L. and Anglada, M., Influencia de la distribución y morfología de las fases en la sensibilidad a fatiga de materiales cerámicos. *Anales de Mecánica de la Fractura*, 1997, **14**, 206–211.
38. Okazaki, M., McEvily, A. J. and Tanaka, T., On the mechanism of fatigue crack growth in silicon nitride. *Metall. Trans*., 1991, **22A**, 1425–1434.